Mechanical behavior, bonding nature and defect processes of Mo2ScAlC2: A new ordered MAX phase

Hadi, MA, Naqib, SH, Christopoulos, S, Chroneos, A & Islam, AKMA

Original citation & hyperlink:
Hadi, MA, Naqib, SH, Christopoulos, S, Chroneos, A & Islam, AKMA 2017, 'Mechanical behavior, bonding nature and defect processes of Mo2ScAlC2: A new ordered MAX phase' *Journal of Alloys and Compounds*, vol 724, pp. 1167-1175
https://dx.doi.org/10.1016/j.jallcom.2017.07.110

DOI 10.1016/j.jallcom.2017.07.110
ISSN 0925-8388
ESSN 1873-4669

Publisher: Elsevier

Mechanical behavior, bonding nature and defect processes of Mo_2ScAlC_2: A new ordered MAX phase

M. A. Hadi[1,a)], S. H. Naqib[1], S.-R. G. Christopoulos,[2] A. Chroneos[2,3,b)], and A. K. M. A. Islam[1,4]

[1]Department of Physics, University of Rajshahi, Rajshahi-6205, Bangladesh
[2]Faculty of Engineering, Environment and Computing, Coventry University, Priory Street, Coventry CV1 5FB, UK
[3]Department of Materials, Imperial College, London SW7 2AZ, UK
[4]International Islamic University Chittagong, 154/A College Road, Chittagong 4203, Bangladesh

Abstract

In the present study, we employed density functional theory calculations to investigate the mechanical behavior, bonding nature and defect processes of the new ordered MAX phase Mo_2ScAlC_2. The mechanical stability of the compound is verified with its single crystal elastic constants. The new phase Mo_2ScAlC_2 is anticipated to be prone to shear along the crystallographic *b* and *c* axes, when a rational force is applied to the crystallographic *a* axis. The compressibility along the ⟨001⟩ direction under uniaxial stress is expected to be easier in Mo_2ScAlC_2. Additionally, the volume deformation should be easier in Mo_2ScAlC_2 than the isostructural Mo_2TiAlC_2. Mo_2ScAlC_2 is predicted to behave in a brittle manner. Due to its higher Debye temperature, Mo_2ScAlC_2 is expected to be thermally more conductive than Mo_2TiAlC_2. The cross-slip pining procedure should be significantly easier in Mo_2ScAlC_2 as compared to Mo_2TiAlC_2. The new ordered MAX phase Mo_2ScAlC_2 has a mixed character of strong covalent and metallic bonding with limited ionic nature. Both Mo–C and Mo–Al bonds are expected to be more covalent in Mo_2ScAlC_2 than those of Mo_2TiAlC_2. The level of covalency of Sc–C bond is somewhat low compared to a similar bond Ti–C in Mo_2ScAlC_2. Due to its reduced hardness Mo_2ScAlC_2, it should be softer and more easily machinable compared to Mo_2TiAlC_2. Fermi surface topology of the new compound is formed mainly due to the low-dispersive Mo 4d-like bands. The intrinsic defect processes reveal that the level of radiation tolerance in Mo_2ScAlC_2 is not as high as in other MAX phases such as Ti_3AlC_2.

Keywords: New MAX phase Mo_2ScAlC_2; Mechanical behavior; Bonding nature; Defect processes

Electronic mail: a) hadipab@gmail.com ;b) alexander.chroneos@imperial.ac.uk

1. Introduction

A class of layered laminated ternary compounds, known as MAX phases with chemical formula $M_{n+1}AX_n$ (M = early transition metal from group 3 – 6, A = element from columns 12 – 16 in the periodic table and X = C and/or N) has gained the interest of the community due to their use and potential for technological applications. For n = 1, 2, 3, the sub-families of these compounds are classified as 211, 312, 413 MAX phases, respectively. In 1960s, Nowotny *et al.* [1] first discovered some members of 211 MAX phases and named them H-phases [1]. MAX phases were revived about two decades ago in 1995 when Barsoum and El-Raghy [2] discovered Ti_3AlC_2 and demonstrated its unique combination of physical and chemical properties inherent to the compounds in the MAX family. These compounds adopt the hexagonal $P6_3/mmc$ structure in which M and X atoms form octahedral edge-sharing building blocks interleaved by A-atomic layers. This structure is highly anisotropic and catalytic for the combination of metallic and ceramic characteristics in MAX phases [3]. The common metallic properties characterized by MAX phases are thermal and electrical conductivities, resistance to thermal shock, plasticity at high temperature, damage tolerance and machinability [2,4–7]. The ceramic-like properties displayed by MAX phases are elastic rigidity, lightweight, creepiness, fatigue, resistance to oxidation and corrosion, maintaining the strength to high temperatures [8–13]. Due to these technologically important properties, MAX phases are already employed in the fields of defense, aerospace, medical, automobile, portable electronics and nuclear reactor [14,15].

About 70 MAX phases have been synthesized in bulk form amongst which only Mo_2GaC, Mo_2TiAlC_2 and $Mo_2Ti_2AlC_3$ contain Mo as the M element. Very recently, Mo_2ScAlC_2 was synthesized by heating the mixture of elemental powders of Mo, Sc, Al and graphite at 1700 °C [16]. The high resolution transmission electron microscopy (HRTEM) study ensures that Mo_2ScAlC_2 is a chemically ordered structure with one Sc layer sandwiched between two Mo-C layers [16]. However, there is only one Sc-based MAX phase Sc_2InC synthesized until now [17,18]. Therefore, the newly synthesized Mo_2ScAlC_2 is an exceptional member in MAX family that combines two uncommon transition metals Mo and Sc as M elements. In the present study, we aim to explore the mechanical and bonding properties of Mo_2ScAlC_2 for the first time including intrinsic defect processes. Additionally, we compare it with the isostructural Mo_2TiAlC_2. The paper is arranged in three sections. In Section 2, a concise description of the computational methodology is presented. The results obtained for the structural, elastic, electronic properties, and intrinsic defect processes of Mo_2ScAlC_2 are analyzed in Section 3. Finally, Section 4 summarizes the main conclusions of the present investigation.

2. Computational methods

The plane wave pseudopotential method within the density functional theory (DFT) as implemented in the CASTEP code [19] is used. The generalized gradient approximation based on Perdew-Burke-Ernzerhof functional (GGA–PBE) [20] is employed to describe the exchange-correlation energy. The Vanderbilt type ultrasoft pseudopotentials with $4s^2 4p^6 4d^5 5s^1$, $3s^2 3p^6 3d^1 4s^2$, $3s^2 3p^1$, and $2s^2 2p^2$ as the basis sets of the valence electron states for Mo, Sc, Al and C, respectively, are chosen to treat the electron-ion interactions [21]. A plane-wave energy cut-off is set as 600 eV for expanding the plane wave functions. The first Brillouin zone is sampled with a 25×25×3 *k*-point mesh according to Monkhorst-Pack (MP) scheme [22]. Broyden-Fletcher-Goldfarb-Shanno (BFGS) algorithm [23] is applied to relax the structure fully with respect to atomic positions and lattice parameters. The tolerance for energy, maximum force, maximum stress, and maximum atomic displacement are chosen to be within 5×10^{-6} eV/atom, 0.01 eV/Å, 0.02 GPa and 5×10^{-4} Å, respectively. The elastic properties are calculated with a 17×17×2 *k*-point mesh and a plane-wave energy cut-off of 550 eV for significantly reducing computational cost.

The elastic constants can be calculated by using the finite-strain theory formulated within CASTEP [24]. In this method, a set of specified uniform deformations (strains) of finite value is applied and after that the consequential stress is evaluated with respect to optimizing the internal degrees of freedom. This method has been used to adequately calculate the elastic properties of many materials including metals [25–34]. The stress tensor σ_{ij} under a set of applied strain δ_j gives the elastic constants via the equation,

$$\sigma_{ij} = \sum_{ij} C_{ij}\delta_j \quad (1)$$

The polycrystalline bulk elastic properties are calculated within the scheme of the Voight-Reuss-Hill (VRH) approximation for polycrystalline aggregates [35–37] by using the calculated elastic constants. The Young's modulus and Poisson's ratio are also determined from the relations $Y = (9GB)/(3B + G)$ and $v = (3B - 2G)/(6B + 2G)$, respectively.

The calculations for the intrinsic defect processes involved a 108-atomic site supercell (under constant pressure conditions) and a 3 x 3 x 1 MP *k*-point grid. For the interstitial sites we performed a comprehensive investigation.

3. Results and discussions

3.1. Structural properties

Mo_2ScAlC_2 crystallizes in a hexagonal structure with the space group of $P6_3/mmc$ like all other MAX phases and is isostructural with Mo_2TiAlC_2. The optimized crystal structure of Mo_2ScAlC_2 is represented in Fig. 1. The k-point and planewave cutoff energy convergence results for structure optimization are shown in Figs. 2. The unit cell of Mo_2ScAlC_2 contains 12 atoms and two formula

units (Z = 2). Table 1 lists the calculated lattice constants *a* and *c* as well as equilibrium unit cell volume together with atomic positions. The DFT results are in good agreement with the experimental values with deviations for lattice constants *a* and *c* and unit cell volume *V* as 0.63, 1.54 and 2.82%, respectively. It can be observed from Table 1 that the exchange of Ti with Sc in Mo_2TiAlC_2 causes an increase in lattice constants and unit cell volume.

Table 1: Structural properties obtained from DFT based first-principles calculations along with corresponding experimental data.

Structural Properties		Experimental data		Theoretical data	
		Mo_2ScAlC_2 [16]	Mo_2TiAlC_2 [38]	Mo_2ScAlC_2 [This]	Mo_2TiAlC_2 [31]
a (Å)		3.0334	2.997	3.0523	2.998
c (Å)		18.7750	18.661	19.0648	18.751
V (Å^3)		149.6132	145.157	153.8176	145.955
Space group		$P6_3/mmc$			
Atomic position					
Mo	4f	(1/3, 2/3, 0.13632)	(1/3, 2/3, 0.13336)	(1/3, 2/3, 0.13709)	(1/3, 2/3, 0.13316)
Sc/Ti	2a	(0, 0, 0)	(0, 0, 0)	(0, 0, 0)	(0, 0, 0)
Al	2b	(0, 0, 1/4)	(0, 0, 1/4)	(0, 0, 1/4)	(0, 0, 1/4)
C	4f	(2/3, 1/3, 0.06825)	(2/3, 1/3, 0.06875)	(2/3, 1/3, 0.07608)	(2/3, 1/3, 0.06857)

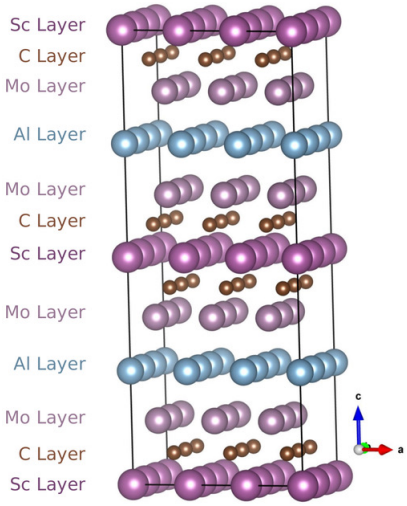

Fig. 1. Crystal structure of chemically ordered MAX phase, Mo_2ScAlC_2.

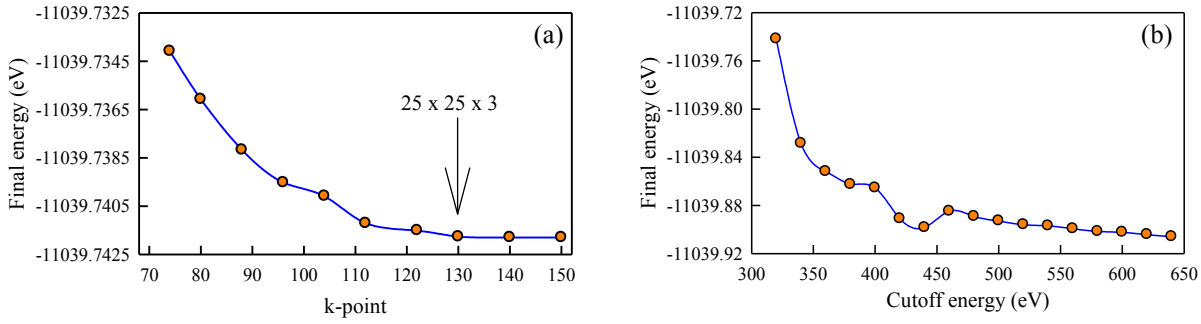

Fig. 2. (a) k-point and (b) planewave cutoff energy convergence results for structure optimization.

3.2. Elastic properties

The mechanical behavior of solids is dependent upon their elastic constants. In particular, elastic constants of solids are related to the bonding characteristics between adjacent atomic planes and the anisotropic nature of the bonding and structural stability. Due to its hexagonal crystal structure, the new ordered MAX phase Mo_2ScAlC_2 has six different elastic constants namely, C_{11}, C_{12}, C_{13}, C_{33}, C_{44}, and C_{66}. Only five of them are independent in view of the fact that $C_{66} = (C_{11} - C_{12})/2$. These independent elastic tensors determine the mechanical stability of the materials. For instance, the mechanical stability of the crystals with hexagonal structure can be assessed with the independent elastic constants via the conditions [39]:

$$C_{11} > 0, \quad C_{33} > 0, \quad C_{44} > 0, \quad (C_{11} - C_{12}) > 0, \text{ and } (C_{11} + C_{12})C_{33} > 2C_{13}^2 \qquad (2)$$

The calculated elastic constants of Mo_2ScAlC_2 are listed in Table 2. All these constants are positive and the above conditions are satisfied, illustrating the mechanical stability of the newly fabricated Mo_2ScAlC_2.

Table 2. Calculated single crystal elastic constants C_{ij} (GPa), polycrystalline bulk modulus B (GPa), shear modulus G (GPa), Young modulus Y (GPa), Pugh's ratio G/B, Poisson's ratio v and shear anisotropy factors A A^U and k_c/k_a of Mo_2ScAlC_2 in comparison with Mo_2TiAlC_2

Compounds	Single crystal elastic properties						Polycrystalline elastic properties								Ref.
	C_{11}	C_{12}	C_{13}	C_{33}	C_{44}	C_{66}	B	G	Y	B/G	v	A	A^U	k_c/k_a	
Mo_2ScAlC_2	293	109	117	290	134	92	173	105	262	1.65	0.25	1.54	0.19	0.97	This
Mo_2TiAlC_2	393	132	133	371	160	131	217	140	346	1.55	0.23	1.29	0.06	1.09	[31]
	386	143	140	367	150	131	220	131	329	1.68	0.25	1.27	0.06	1.10	[40]

The elastic stiffness of a material regarding the (100)⟨100⟩ uniaxial strain can be estimated by its elastic constant C_{11}. It is observed that the replacement of Ti with Sc decreases the stiffness of Mo_2ScAlC_2. It is, therefore, expected that the new phase Mo_2ScAlC_2 should be softer and more easily machinable than Mo_2TiAlC_2. The independent elastic constants C_{12} and C_{44} are linked to the elasticity in shape. In particular, the elastic tensor C_{12} is related to the pure shear stress in the (110) plane along the ⟨100⟩ direction, whereas the elastic constant C_{44} is caused by the shear stress in the (010) plane in the ⟨001⟩ direction. The shear deformations associated with these two shear stresses are expected to be easier in Mo_2ScAlC_2 than in Mo_2TiAlC_2. The elastic constants C_{12} and C_{13} combine a functional stress component along the crystallographic a direction in the presence of a uniaxial strain along the crystallographic b and c axes, uniformly. Due to low values of these constants in comparison with those of Mo_2TiAlC_2, the new compound Mo_2ScAlC_2 is expected to be prone to shear along the crystallographic b and c axes, when a reasonable force is applied to the crystallographic a axis. The independent elastic tensor C_{33} is due to the uniaxial deformation along the ⟨001⟩ direction. The substitution of Ti from Mo_2TiAlC_2 with Sc causes a decrease of C_{33} and consequently, the compressibility along the ⟨001⟩ direction under uniaxial stress is expected to be easier in Mo_2ScAlC_2.

The bulk elastic parameters are calculated and listed in Table 3. The bulk modulus B measures the aptitude of solids to resist compression. It also reflects the nature of chemical bonding within a solid. The replacement of Ti with Sc causes a significant decrease in bulk modulus of Mo_2ScAlC_2. Therefore, the volume deformation is expected to be easier in Mo_2ScAlC_2 than in Mo_2TiAlC_2. Moreover, the strength of chemical bonding in Mo_2ScAlC_2 is low as compared to Mo_2TiAlC_2. All these signify that the new phase Mo_2ScAlC_2 is softer than Mo_2TiAlC_2. The shear modulus G assesses the materials' ability to resist their plastic deformation i.e., shape change. It also correlates with hardness and the elastic constant C_{44}. It is observed that the shear modulus decreases significantly when the Ti atom is replaced with Sc from Mo_2TiAlC_2. Therefore, the shape change in Mo_2TiAlC_2 should not be as easy as in Mo_2ScAlC_2, which also implies that Mo_2ScAlC_2 is more easily machinable than Mo_2TiAlC_2. The Young's modulus Y is a measure of the stiffness of a solid material, with a stiff material requiring more force to deform as compared to a soft material. A remarkable decrease is observed in Young's modulus when comparing Mo_2TiAlC_2 to Mo_2ScAlC_2, indicating that in view of Young's modulus the new compound Mo_2ScAlC_2 should also be softer than Mo_2TiAlC_2.

The failure mode of solids (brittle or ductile failure) can be explained depending on their bulk and shear modulus. This is of importance to determine the integrity of the structure. A sudden fracture appears in a material due its brittle failure; conversely plastic deformation occurs before fracture for a material that undergoes ductile failure. In ductile failure, the crack progresses slowly with a large amount of plastic deformation and it will typically not spread unless an increased stress is applied. Conversely, in brittle failure, cracks extend very rapidly with little or no plastic deformation. Pugh [41] used the bulk to shear modulus ratio B/G as a parameter to determine whether a material is brittle or ductile. The critical value of 1.75 for B/G is the borderline between ductile and brittle materials [41], with brittle materials being below and ductile materials exceeding the critical value. Considering this criterion Mo_2ScAlC_2 should behave like a brittle material as its B/G = 1.65.

Poisson's ratio v is a very important parameter that provides information regarding the characteristics of the bonding. Poisson's ratio classifies solid materials into two groups: central force solids and non-central force solids [42]. For central force solids, the Poisson's ratio ranges from 0.25 to 0.50. A material is classified as a non-central force solid if its Poisson's ratio is either less than 0.25 or greater than 0.50. The calculated value of v for the new layered compound Mo_2ScAlC_2 is 0.25, implying that it should be a central force solid like its isostructural Mo_2TiAlC_2 [40]. The Poisson's ratio is also used to quantify the failure mode of solids. The threshold value of this parameter, v = 0.26 [43,44] separates the brittle from ductile materials. The values less than the threshold value correspond to a brittle material and the values greater than threshold value is associated with a ductile material. In view of Poisson's ratio, Mo_2ScAlC_2 is brittle in nature in agreement with the calculated Pugh's ratio. Poisson's ratio is a useful tool to predict the nature of chemical bonding in solids. With v = 1.0, a material is classified as a covalent solid, whereas v = 0.33 corresponds to a metallic material

[45]. Mo_2ScAlC_2 is therefore expected to be characterized by a mixture of covalent and metallic properties.

A practically important topic concerns a body that cannot develop the same strain independently of the direction in which stress is applied (elastically anisotropic). In nature, there are no crystalline solids that violate this type of behavior and a deeper understanding of such anisotropic behavior is, important in crystal physics and engineering. An elastic anisotropy factor seeks to quantify how directionally dependent the elastic properties of a system are. Elastic anisotropy also leads to the anisotropy of thermal expansion and microcracks in the crystal [46]. For this reason, it is essential to study the elastic anisotropy to discover the mechanisms that improve the durability of materials. Among different anisotropy factors, the shear anisotropy index owns importance by quantifying the anisotropy in the bonding between atoms in different planes. For hexagonal crystals, this factor is defined by $A = 4C_{44}/(C_{11} + C_{33} - 2C_{13})$ and is coupled with the {100} shear planes between the ⟨011⟩ and ⟨010⟩ directions. To be isotropic, a hexagonal crystal must have anisotropy factor $A = 1$. With A-value less than or greater than unity, a crystal exhibits anisotropy in its elastic properties. The amount of deviation from unity quantifies the level of anisotropy possessed by the crystal for its elastic properties. The large A-value makes possible the driving force (tangential force) acting on the screw dislocations to progress the cross-slip pinning process [47]. The A-value of Mo_2ScAlC_2 deviates more than that of Mo_2TiAlC_2 from unity, indicating that the elastic anisotropy is profound in Sc-based Mo_2ScAlC_2. The cross-slip pining process is significantly easier to promote in Mo_2ScAlC_2 but not in Mo_2TiAlC_2. We have also calculated the universal anisotropy factor A^U introduced by Ranganathan and Ostoja-Starzewski [48]: $A^U = 5(G_V/G_R) + (B_V/B_R) - 6 \geq 0$. This index attains zero value for an isotropic material and any value being greater than zero indicates the level of anisotropy. The obtained value of 0.19 also signifies the considerable anisotropy of Mo_2ScAlC_2 compared to the isostructural Mo_2TiAlC_2. Another anisotropy factor defined by the ratio between the linear compressibility coefficients along the c- and a-axis: $k_c/k_a = (C_{11} + C_{12} - 2C_{13})/(C_{33} - C_{13})$ is calculated. The results indicate that the compressibility along the c-axis is slightly smaller than that along the a-axis in Mo_2ScAlC_2, whereas the compressibility along the c-axis is slightly larger than that along the a-axis for Mo_2TiAlC_2. In fact, Mo_2ScAlC_2 is more incompressible along the c-axis compared with Mo_2TiAlC_2.

Mechanical wave velocity and Debye temperature

The elastic moduli of a solid links the Debye temperature and the mechanical wave (sound wave) velocity with which it travels through the solid. The transverse and longitudinal velocity of sound traversing through a crystalline solid with bulk modulus B and shear modulus G can be obtained from [49]:

$$v_t = \left[\frac{G}{\rho}\right]^{1/2} \quad \text{and} \quad v_l = \left[\frac{3B + 4G}{\rho}\right]^{1/2} \tag{3}$$

where ρ refers to the mass-density of the solid. The average sound velocity v_m can be evaluated from the transverse and longitudinal sound velocities using [49]:

$$v_m = \left[\frac{1}{3}\left(\frac{1}{v_l^3} + \frac{2}{v_t^3}\right)\right]^{-1/3} \quad (4)$$

The average sound velocity is subsequently linked to the one of the standard methods to determine the Debye temperature via [49]:

$$\theta_D = \frac{h}{k_B}\left[\left(\frac{3n}{4\pi}\right)\frac{N_A\rho}{M}\right]^{1/3} v_m \quad (5)$$

where h denotes the Planck's constant, k_B is Boltzmann's constant, N_A refers to Avogadro's number, M defines the molecular weight and n is the number of atoms in the molecule.

Table 3. Calculated density (ρ in gm/cm^3), longitudinal, transverse and average sound velocities (v_l, v_t, and v_m in km/s) and Debye temperature (θ_D in K) of Mo_2ScAlC_2 in comparison with Mo_2TiAlC_2.

Compounds	ρ	v_l	v_t	v_m	θ_D	Ref.
Mo_2ScAlC_2	6.375	12.136	4.058	4.617	592.7	This
Mo_2TiAlC_2	6.297	8.006	4.715	3.196	413.6	[31]

The calculated mechanical wave velocities and Debye temperature are reported in Table 3. The longitudinal and average sound velocities are found to increase, though the transverse sound velocity decreases with the replacement of Ti by Sc. The Debye temperature increases following the average sound velocity as θ_D is directly proportional to v_m. As a general rule, a higher Debye temperature is associated to a higher phonon thermal conductivity. Therefore, Mo_2ScAlC_2 should be thermally more conductive than Mo_2TiAlC_2.

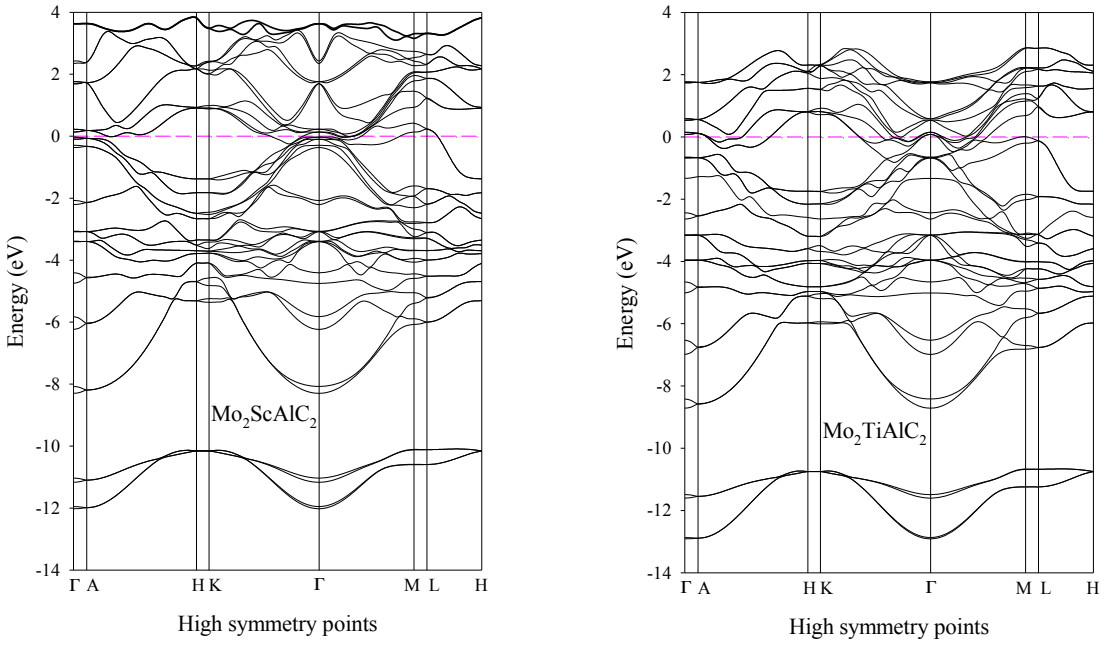

Fig. 3. Electronic band structure of ordered MAX phases Mo_2ScAlC_2 and Mo_2TiAlC_2.

3.3. Electronic properties

The bonding nature of a solid can be described with its electronic properties i.e., band structure, density of states (DOS), Mulliken atomic populations, total charge density and Fermi surface. The calculated band structure of Mo_2ScAlC_2 is shown in Fig. 3 along with the band structure of Mo_2TiAlC_2 [31]. Although the band profiles of these two isostructural ordered MAX phases are similar, there are some distinct differences between them. The metallic bonding exists within both compounds due to the overlapping of conduction bands with valence bands, therefore no band gap is observed at the Fermi level of both nanolaminates. The Fermi surface of Mo_2ScAlC_2 appears just above the valence band maximum near the Γ point, whereas the Fermi surface of Mo_2TiAlC_2 becomes visible just below the valence bands maximum close to the Γ point. The conduction bands of Mo_2ScAlC_2 are wider than those of Mo_2TiAlC_2. Conversely, the lowest lying valence bands of Mo_2ScAlC_2 are rather narrow in comparison with those of Mo_2TiAlC_2. Comparatively, a higher number of valence bands of Mo_2ScAlC_2 assemble at Fermi level around the Γ point. The overlapping between the valence and conduction bands is more significant in Mo_2ScAlC_2 compared to Mo_2TiAlC_2. Therefore, it is expected that Mo_2ScAlC_2 should be more conductive than Mo_2TiAlC_2.

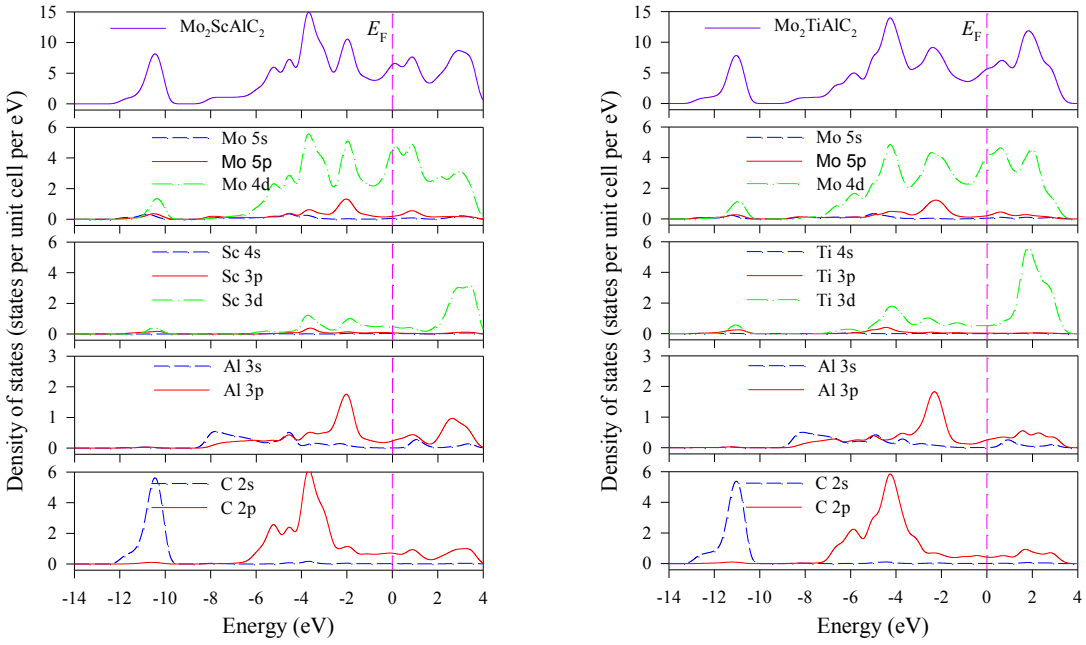

Fig. 4. Density of states of ordered MAX phases Mo_2ScAlC_2 and Mo_2TiAlC_2.

The DOS provide insights into the chemical bonding in crystals. The calculated total and partial DOS of Mo_2ScAlC_2 are shown in Fig. 4 together with those of Mo_2TiAlC_2 [31] to facilitate comparison. In both phases, the most of the states at the Fermi energy E_F comes from the d-orbitals of the transition metal Mo. These d-resonances at the vicinity of the Fermi level make the two nanolaminates electrically conductive. The calculated total DOS at the Fermi levels $N(E_F)$ are found to be 6.5 and 5.6

eV for Mo_2ScAlC_2, and Mo_2TiAlC_2, respectively, indicating that the level of metallic conductivity is expected to be high in Mo_2ScAlC_2 in comparison to Mo_2TiAlC_2. The lowest valence band in both ordered MAX phases situated between -13.1 eV and -9.5 eV arises due to hybridization between s-orbitals of C and d-orbitals of Mo as well as Sc/Ti. As a result, covalent bonding between transition metals and C is developed. In both phases the Mo–C bond should be stronger than the other bond Sc–C/Ti–C because of high density of Mo d-states. The higher valence band of Mo_2ScAlC_2 consists of four distinct peaks, whereas the valence band of Mo_2TiAlC_2 contains three distinct peaks. The additional peak of Mo_2ScAlC_2 is due to the hybridization of C 2p states with Mo 4d states. The peak at the left of the highest peak in both MAX phases originates from the hybridization between C 2p and Mo 4d states. The highest peak consists of the leading contribution from C 2p and Mo 4d states with a small contribution from Sc/Ti 3d states. The peak at the right of the highest peak arises due to the hybridization of Al 3p orbitals with Mo 4d/5p orbitals. This hybridization leads to the formation of the Mo-Al bond, which is weaker than both Mo–C and Ti-C bonds due to the position near Fermi level. To summarize, it can be concluded that Mo_2ScAlC_2 has a mixed character of strong covalent and metallic bonding. Commonly, to most MAX phases it also contains some ionic nature because of the difference in electronegativity between the constituting elements.

Mulliken atomic population and Vickers hardness

Mulliken atomic populations are largely based on first-order electron density functions within a linear combination of atomic orbitals-molecular orbital (LCAO- MO) theory [50]. Mulliken population analysis assesses the distribution of electrons in several fractional means among the different parts of atomic bonds. In addition, the overlap population abides a good relation with covalency of bonding and bond strength [51]. Moreover, the overlap population is a convenient way to measure the potency of chemical bonding in DFT calculations [52]. However, Mulliken atomic population analysis is not applicable with the CASTEP code as the DFT method is formulated based on a plane-wave basis set that provides no straightforward way to compute the local atomic properties. Sanchez-Portal *et al.* [53] made the CASTEP code to be suitable for Mulliken atomic populations with a technique in which a projection of plane-wave states onto a linear combination of atomic orbitals (LCAO) is used. The atomic charges and the bond populations can be obtained from Mulliken atomic population analysis. The Mulliken charge associated with a particular atom α can be calculated as [50]:

$$Q(\alpha) = \sum_{\mathrm{k}} w_{\mathrm{k}} \sum_{\mu}^{on\ \alpha} \sum_{\nu} P_{\mu\nu}(\mathrm{k}) S_{\mu\nu}(\mathrm{k}) \tag{6}$$

The overlap population between two atoms α and β can be expressed as [50]:

$$P(\alpha\beta) = \sum_{\mathrm{k}} w_{\mathrm{k}} \sum_{\mu}^{on\ \alpha} \sum_{\nu}^{on\ \beta} 2P_{\mu\nu}(\mathrm{k}) S_{\mu\nu}(\mathrm{k}) \tag{7}$$

where $P_{\mu\nu}$ refers to an element of the density matrix and $S_{\mu\nu}$ denotes the overlap matrix. The nature of chemical bonding in crystalline solids can be realized with the knowledge of effective valence charge and Mulliken atomic population. The effective valence charge is estimated from the difference between the formal ionic charge and Mulliken charge on the anion species in a crystal. The identity of a chemical bond either as covalent or ionic with its strength can be determined with the effective valence. The zero effective valences are associated with a purely ionic bond, while the values greater than zero indicate the increasing levels of covalency. The calculated effective valences listed in Table 4 imply that the two isostructural ordered MAX phases include chemical bonding with prominent covalency.

Table 4. Population analysis of Mo_2ScAlC_2 and Mo_2TiAlC_2 [31].

Compounds	Species	Mulliken Atomic populations					Effective valence Charge (e)
		S	P	D	Total	Charge (e)	
Mo_2ScAlC_2	C	1.48	3.18	0.00	4.66	– 0.66	--
	Al	0.91	1.76	0.00	2.67	0.33	2.67
	Sc	1.99	6.36	1.69	10.04	0.96	2.04
	Mo	2.27	6.72	5.00	13.99	0.10	5.90
Mo_2TiAlC_2	C	1.45	3.19	0.00	4.64	– 0.64	--
	Al	0.91	1.79	0.00	2.70	0.30	2.70
	Ti	2.04	6.45	2.64	11.12	0.88	2.12
	Mo	2.23	6.70	5.02	13.95	0.05	5.95

Table 5. Calculated Mulliken bond number n_μ, bond length d_μ, bond overlap population P_μ, bond volume v_b^μ and bond hardness H_v^μ of μ-type bond and metallic population $P_{\mu'}$ and Vickers hardness H_v of Mo_2ScAlC_2 and Mo_2TiAlC_2 [31].

Compounds	Bond	n_μ	d_μ (Å)	P_μ	$P_{\mu'}$	v_b^μ (Å^3)	H_v^μ (GPa)	H_v (GPa)
Mo_2ScAlC_2	Mo–C	4	2.11152	1.45	0.024	8.4525	30.09	8.03
	Sc–C	4	2.28232	0.51	0.024	10.6741	6.95	
	Mo–Al	4	2.78194	0.49	0.024	19.3305	2.48	
Mo_2TiAlC_2	Mo-C	4	2.11238	1.21	0.025	8.3452	25.54	9.01
	Ti-C	4	2.15599	0.76	0.025	8.8727	14.30	
	Mo-Al	4	2.79205	0.40	0.025	19.2709	2.00	

The calculated bond overlap populations for only nearest neighbors in the ordered new MAX phase compound are presented in Table 5. The overlap population of nearly zero value indicates that the interaction between the electronic populations of the two atoms is insignificant and a bond with the smallest Mulliken population is extremely weak and can be ignored to calculate the materials' hardness. A high degree of ionicity is observed to be associated with a low overlap population. Conversely, a high value is an indication of a high degree of covalency in the chemical bond. The positive and negative bond overlap populations are due to the bonding and antibonding states, respectively. It is observed that both Mo–C and Mo–Al bonds are more covalent in Mo_2ScAlC_2 than in Mo_2TiAlC_2. The degree of covalency of Sc–C bond is slightly low compared to its similar bond Ti–C.

The prediction of hardness with Mulliken population using DFT is of interest. Gao [54] developed a formula that can successfully calculate the Vickers hardness of non-metallic compounds. Due to delocalized metallic bonding the metallic and semi-metallic compounds cannot be described with this formalism [55]. Making a correction due to such bonding Gou *et al.* [56] proposed the following relation for metallic compounds:

$$H_v^{\mu} = 740\left(P^{\mu} - P^{\mu'}\right)(v_b^{\mu})^{-5/3} \tag{8}$$

where P^{μ} refers to the Mulliken overlap population of the μ-type bond, $P^{\mu'}$ is the metallic population and is calculated from the cell volume V and the number of free electrons in a cell $n_{free} = \int_{E_P}^{E_F} N(E)dE$ as $P^{\mu'} = n_{free}/V$, and v_b^{μ} refers the volume of a bond of μ-type that is evaluated from the bond length $d^{\mu}$of type μ and the number of bonds N_b^{υ} of type ν per unit volume as $v_b^{\mu} = (d^{\mu})^3/\sum_{\nu}[(d^{\mu})^3 N_b^{\nu}]$. The hardness of a complex multiband crystal can be obtained from the geometric average of all individual bond hardness [57,58]:

$$H_V = [\overset{\mu}{\Pi}(H_v^{\mu})^{n^{\mu}}]^{1/\sum n^{\mu}} \tag{9}$$

where n^{μ} is the number of bond of type μ that composes the real multiband crystals. The calculated Vickers hardness of Mo_2ScAlC_2 along with its analogue Mo_2TiAlC_2 is listed in Table 5. The H_V value of 8.03 GPa for Mo_2ScAlC_2 is calculated to be smaller compared to 9.01 GPa for Mo_2TiAlC_2. It is clear that the replacement of Ti with Sc reduces the hardness of Mo_2ScAlC_2 and makes it relatively soft and easily machinable compared to Mo_2TiAlC_2.

Charge density

The electron charge density distribution of Mo_2ScAlC_2 is investigated to obtain further insights into the chemical bonding. The contour of calculated electron charge density in the $(11\bar{2}0)$ plane is shown in Fig. 5. The atom of high electronic charge i.e., electronegativity pulls electron density towards itself [59]. The electron charge density map discloses a strong directional Mo–C–Mo covalent bond chain with each pair of the chain coupled with a comparatively weak Sc–C bond. The directional M–X–M covalent bonding is common feature in MAX phases [60]. Due to a large variation in electronegativity, the electronic charge in the vicinity of Mo atoms is attracted towards C atoms. Consequently, a strong covalent-ionic bonding along Mo and C direction is induced. This bond arises due to hybridization between C 2s and Mo 4d electrons. Relatively weak Mo-Al bonds form as the electron charge density of Mo atom just overlaps with that of the Al atom. The present results are consistent with the findings that MAX phases typically have reasonably strong M–X bonds and relatively weak M–A bonds [3].

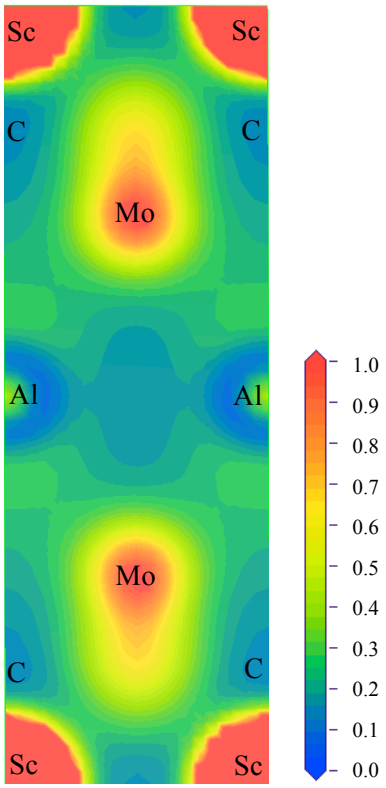

Fig. 5. Electronic charge density in $(11\bar{2}0)$ plane of Mo_2ScAlC_2. The scale indicates the low and high electron density with blue and red color, respectively.

3.4. Intrinsic defect processes

Frenkel defect formation

The energetics of intrinsic defect process and in particular the Frenkel defects can be important to access the radiation tolerance of materials. Considering for example nuclear applications a low pair formation energy may be linked with a higher content of more persistent defects. These in turn may lead to the loss of ordering in the crystal. The following relations are the key Frenkel reactions in Kröger–Vink notation (here V_A and A_i denote a vacant A site and an A interstitial defect respectively) [61]:

$$M_M \rightarrow V_M + M_i \quad (10)$$

$$A_A \rightarrow V_A + A_i \quad (11)$$

$$X_X \rightarrow V_X + X_i \quad (12)$$

As it has been previously [62] discussed in 312 MAX phases there are numerous possible interstitial sites. The calculated energetically preferable interstitials sites are: Mo_i (3/4, 0.636, 1/4), Sc_i (0.764, 0.699, 1/4), Al_i (2/3, 1/3, 1/4) and C_i (0.340, 2/3, 1/4).

Antisite defect formation

During radiation damage the produced point defects may either recombine or reside on alternative lattice site forming antisite defects [63]. From a physical viewpoint a low energy antisite formation energy means that a high proportion of residual defects will remain in the material as typically the conversion of an interstitial into an antisite will result to a net reduction of defect mobility [63]. The antisite formation mechanisms are:

$$M_M + A_A \rightarrow M_A + A_M \quad (13)$$

$$M_M + X_X \rightarrow M_X + X_M \quad (14)$$

$$A_A + X_X \rightarrow A_X + X_A \quad (15)$$

Table 6. The calculated defect reaction energies (in eV, for relations 10-15) for the Mo_2ScAlC_2 MAX phase.

Reaction	Frenkel	Reaction	Antisite
$Mo_{Mo} \rightarrow V_{Mo} + Mo_i$	6.393	$Mo_{Mo} + Al_{Al} \rightarrow Mo_{Al} + Al_{Mo}$	2.866
$Sc_{Sc} \rightarrow V_{Sc} + Sc_i$	8.494	$Mo_{Mo} + C_C \rightarrow Mo_C + C_{Mo}$	9.106
$Al_{Al} \rightarrow V_{Al} + Al_i$	4.656	$Sc_{Sc} + Al_{Al} \rightarrow Sc_{Al} + Al_{Sc}$	2.835
$C_C \rightarrow V_C + C_i$	2.503	$Sc_{Sc} + C_C \rightarrow Sc_C + C_{Sc}$	11.995
		$Al_{Al} + C_C \rightarrow Al_C + C_{Al}$	8.386

Implications of defect processes

The radiation performance of materials is dependent upon their propensity to form and accommodate point defects [62,63]. A high concentration of defects may lead to the destabilization of the MAX phase (or any material) and may result to volume changes and microcracking [63-66]. It is established that displacive radiation can result to an athermal concentration of Frenkel pairs and therefore the radiation tolerance of materials is linked to their ability to resist the formation of significant populations of Frenkel and/or antisite) defects. Therefore, high Frenkel and antisite defect energies may be considered as a condition of radiation tolerance.

As it can be observed from Table 6 which is based on the defect processes investigated by DFT the dominant intrinsic defect mechanism is the carbon Frenkel energy (2.503 eV). Additionally, antisite processes could lead to the formation of $Mo_{Al} + Al_{Mo}$ (2.866 eV) and $Sc_{Al} + Al_{Sc}$ (2.835 eV). It can be concluded from these results that other MAX phases such as Ti_3AlC_2 [60,61] is more radiation tolerant than Mo_2ScAlC_2.

4. Concluding remarks

To summarize, the mechanical behavior, bonding nature and defect processes of Mo_2ScAlC_2 is calculated using DFT for the first time. To facilitate comparison we consider the isostructural

Mo_2TiAlC_2 MAX phase. The relaxed structural parameters are in good agreement with the experimental results. The calculated single crystal elastic constants ensure the mechanical stability of the compound. Mo_2ScAlC_2 is calculated to be prone to shear along the crystallographic *b* and *c* axes, when an eligible force is applied to the crystallographic *a* axis. Under uniaxial stress, the compressibility along the ⟨001⟩ direction is predicted to be easier in Mo_2ScAlC_2. The volume deformation is expected to be easier in Mo_2ScAlC_2 than in Mo_2TiAlC_2. The new compound should behave in a brittle manner. The high Debye temperature of Mo_2ScAlC_2 indicates its higher thermal conductivity than Mo_2TiAlC_2. The cross-slip pining process is easier to promote in Mo_2ScAlC_2 than in Mo_2TiAlC_2. The chemical bonding in Mo_2ScAlC_2 is a mixture of strong covalent and metallic with little ionic nature. Bonds Mo–C and Mo–Al should be more covalent in Mo_2ScAlC_2 than those in Mo_2TiAlC_2. The degree of covalency of Sc–C bond is rather low compared to the Ti–C bond. Due to its low hardness Mo_2ScAlC_2 is expected to be softer and more easily machinable compared to Mo_2TiAlC_2. The low-dispersive Mo 4d-like bands should be responsible to form the Fermi surface topology of the new compound. The carbon Frenkel defect reaction is the lowest energy intrinsic defect process in Mo_2ScAlC_2. The level of radiation tolerance in Mo_2ScAlC_2 is evaluated to be relatively low compared to other MAX phases such as Ti_3AlC_2.

Acknowledgements

S.R.G.C. and A.C. are grateful for funding from the Lloyd's Register Foundation, a charitable foundation helping to protect life and property by supporting engineering-related education, public engagement and the application of research.

References

[1] W. Jeitschko, H. Nowotny and F. Benesovsky, Monatsh. Chem. 94 (1963) 672.

[2] M.W. Barsoum and T. El-Raghy, J. Am. Ceram. Soc. 79 (1996) 1953.

[3] M. W. Barsoum, Prog. Solid State Chem. 28 (2001) 201.

[4] H. Yoo, M. W. Barsoum and T. El-Raghy, Nature (London) 407 (2000) 581.

[5] T. El-Raghy *et al.*, J. Am. Ceram. Soc. 82 (1999) 2855.

[6] M.W. Barsoum, L. Farber and T. El-Raghy, Metall. Mater. Trans. A 30 (1999) 1727.

[7] Z. M. Sun *et al.*, Mater. Trans. 47 (2006) 170.

[8] P. Finkel, M. W. Barsoum and T. El-Raghy, J. Appl. Phys. 87 (2000) 1701.

[9] M. W. Barsoum, Physical properties of the MAX phases, *Encyclopedia of Materials: Science and Technology* (Elsevier, Amsterdam, 2009).

[10] M. Radovic *et al.*, J. Alloys Compds. 361 (2003) 299.

[11] C. J. Gilbert *et al.*, Scr. Mater. 238 (2000) 761.

[12] M. Sundberg *et al.*, Ceram. Int. 30 (2004) 1899.

[13] D. Horlait, S. Grasso, A. Chroneos, and W. E. Lee, Mater. Res. Lett. 4 (2016) 317.

[14] S. E. Lofland, J. D. Hettinger, K. Harrell, P. Finkel, S. Gupta, M. W. Barsoum, and G. Hug, Appl. Phys. Lett. 84 (2004) 508.

[15] D. Horlait, S. C. Middleburgh, A. Chroneos and W. E. Lee, Sci. Rep. 6 (2016) 18829.

[16] R. Meshkian, Q. Tao, M. Dahlqvist, J. Lu, L. Hultman, and J. Rosen, Acta Materialia 125 (2017) 476.

[17] H. Nowotny, Strukturchemie einiger verbindungen der übergangsmetalle mitden elementen C, Si, Ge, Sn, Prog. Solid. State. Chem. 5 (1971) 27.

[18] L.E. Toth, W. Jeitschko, C.M. Yen, The superconducting behavior of several complex carbides and nitrides, J. Less Common Metals 10 (1966) 29.

[19] S. J. Clark, M. D. Segall, C. J. Pickard, P. J. Hasnip, M. I. J. Probert, K. Refson, and M. C. Payne, Zeitschrift für Kristallographie 220 (2005) 567.

[20] J. P. Perdew, K. Burke, and M. Ernzerhof, Phys. Rev. Lett. **77** (1996) 3865.

[21] D. Vanderbilt, Phys. Rev. B 41(1990) 7892.

[22] H. J. Monkhorst, J. D. Pack, Phys. Rev. B 13 (1976) 5188.

[23] T. H. Fischer and J. Almlof, J. Phys. Chem. 96 (1992) 9768.

[24] F. D. Murnaghan, Finite Deformation of an Elastic Solid (Wiley, New York, 1951).

[25] M. A. Hadi, M. Roknuzzaman, F. Pervin, S. H. Naqib, A. K. M. A. Islam and M. Aftabuzzaman, J. Sci. Res. 6 (2014) 11.

[26] M. T. Nasir, M. A. Hadi, S. H. Naqib, F. Pervin, A. K. M. A. Islam, M. Roknuzzaman, and M. S. Ali, Int. J. Mod. Phys. B 28 (2014) 1550022.

[27] M. Roknuzzaman, M. A. Hadi, M. J. Abden, M. T. Nasir, A. K. M. A. Islam, M. S. Ali, K. Ostrikov, and S. H. Naqib, Comp. Mater. Sci. 113 (2016) 146.

[28] M. A. Hadi, Comp. Mater. Sci. 117 (2016) 422.

[29] M. A. Hadi, M. A. Alam, M. Roknuzzaman, M. T. Nasir, A. K. M. A. Islama, and S. H. Naqib, Chin. Phys. B 24 (2015) 117401.

[30] M. A. Alam, M. A. Hadi, M. T. Nasir, M. Roknuzzaman, F. Parvin, M. A. K. Zilani, A. K. M. A. Islam, S. H. Naqib, J. Supercond. Nov. Magn. 29 (2016) 2503.

[31] M. A. Hadi and M. S. Ali, Chin. Phys. B 25 (2016) 107103.

[32] M. A. Hadi, M. T. Nasir, M. Roknuzzaman, M. A. Rayhan, S. H. Naqib, and A. K. M. A. Islam, Phys. Status Solidi B, 253 (2016) 2020.

[33] M. A. Hadi, M. S. Ali, S. H. Naqib and A. K. M. A. Islam, Chinese Physics B 26 (2017) acceptd.

[34] M. H. K. Rubel, M. A. Hadi, M. M. Rahaman, M. S. Ali, M. Aftabuzzaman, R. Pervin, A. K. M. A. Islam, and N. Kumada, Comp. Mater. Sci. (2017) submitted.

[35] W. Voigt, *Lehrbuch der Kristallphysik*, (Taubner, Leipzig, 1928).

[36] A. Reuss and Z. Angew, Math. Mech. 9 (1929) 49.

[37] R. Hill, Proc. Phys. Soc. A 65 (1952) 349.

[38] B. Anasori, J. Halim, J. Lu, A. Cooper, Voigt, L. Hultman and M. W. Barsoum, Scripta Materialia 101 (2015) 5.

[39] M. Born, Math. Proc. Cambridge Philos. Soc. 36 (1940) 160.

[40] B. Anasori, M. Dahlqvist, J. Halim, E. J. Moon, J. Lu, B. C. Hosler, E. N. Caspi, S. J. May, L. Hultman,P. Eklund, J. Rose′n, and M. W. Barsoum, J. Appl. Phys. 118 (2015) 094304.

[41] S.F. Pugh, Phil. Mag. 45 (1954) 823.

[42] O. L. Anderson and H. H. Demarest Jr., J. Geophys. Res. 76 (1971) 1349.

[43] I. N. Frantsevich, F. F. Voronov, and S.A. Bokuta, Elastic constants and elastic moduli of metals and insulators handbook, (Naukova Dumka, Kiev, 1983, pp. 60–180).

[44] G. Vaitheeswaran, V. Kanchana, A. Svane and A. Delin, J. Phys.: Conden. Matter 19 (2007) 326214.

[45] A. Savin, D.C.H. Flad, J. Flad, H. Preuss, H.G. Schnering, Angew. Chem. Int. Ed. Engl. 31 (1992) 185.

[46] V. Tvergaard and J. W. Hutchinson, J. Am. Chem. Soc. 71 (1988) 157.

[47] M. H. Yoo, Scr. Metall. 20 (1986) 915.

[48] S.I. Ranganathan, M. Ostoja-Starzewski, Phys. Rev. Lett. 101 (2008) 055504.

[49] E. Schreiber, O. L. Anderson, N. Soga, Elastic Constants and Their Measurements (McGraw-Hill, New York, 1973)

[50] R. S. Mulliken, J. Chem. Phys. 23 (1955) 1833.

[51] M. D. Segall *et al.*, Phys. Rev. B 54 (1996) 16317.

[52] W. Y. Ching and Y. N. Xu, Phys. Rev. B 59 (1999) 12815.

[53] D. Sanchez-Portal, E. Artacho, and J. M. Soler, Solid State Commun. 95 (1995) 685.

[54] F. M. Gao, Phys. Rev. B 73 132104 (2006).

[55] J. H. Westbrook and H. Conrad, The Science of Hardness Testing and Its Research Applications (ASM, Ohio, 1973).

[56] H. Gou, L. Hou, J. Zhang and F. Gao, Appl. Phys. Lett. 92 241901 (2008).

[57] A. Szymański and J. M. Szymański, Hardness Estimation of Minerals Rocks and Ceramic Materials, 6th edition, (Elsevier, Amsterdam, 1989).

[58] V. M. Glazov and V. N. Vigdorovid, Hardness of Metals (Izd. Metellurgiya, Moskva, 1989).

[59] IUPAC 1997 Compendium of Chemical Technology, 2nd edn. (the “Gold Book”); 2006 Online corrected version.

[60] J. Phys.: Condens. Matter **12** (2000) L457–L462.

[61] F. A. Kröger and H. J. Vink, Solid State Phys. 3 (1956) 307.

[62] E. Zapata-Solvas, S.-R. G. Christopoulos, N. Ni, D. C. Parfitt, D. Horlait, M. E. Fitzpatrick, A. Chroneos, and W. E. Lee, J. Am. Ceram. Soc. 100 (2017) 1377.

[63] S. C. Middleburgh, G. R. Lumpkin, and D. Riley, J. Am. Ceram. Soc. 96 (2013) 3196.

[64] W. J. Weber, Radiat. Eff. 77 (1983) 295.

[65] F. W. Clinard Jr, D. L. Rohr, and R. B. Roof, Nucl. Instrum. Methods Phys. Res. B 1 (1984) 581.

[66] E. Zapata-Solvas, M. A. Hadi, D. Horlait, D. C. Parfitt, A. Thibaud, A. Chroneos, and W. E. Lee, J. Am. Ceram. Soc. DOI: 10.1111/jace.14870